J Electr Eng Technol.2018; 13(1): 352-361
http://doi.org/10.5370/JEET.2018.13.1.352

ISSN(Print) 1975-0102
ISSN(Online) 2093-7423

# A Sensing System of the Halbach Array Permanent Magnet Spherical Motor Based on 3-D Hall Sensor

**Hongfeng Li*, Wenjun Liu† and Bin Li***

**Abstract** – This paper proposes a sensing system of the Halbach array permanent magnet spherical motor(PMSM). The rotor position can be obtained by solving three rotation angles, which revolves around 3 reference axes of the stator. With the development of 3-D hall sensor, the position identification problem of the Halbach array PMSM based on rotor magnetic field is studied in this paper. A nonlinear and serious coupling relationship between the rotation angles and the measured magnetic flux density is established on the basis of the rotation transformation theory and the magnetic field model. In order to get rid of the influence on position detection caused by the harmonics of rotor magnetic field and the stator coil magnetic field, a sensor location combination scheme is proposed. In order to solve the nonlinear equation fast and accurately, a new position solution algorithm which combines the merits of gradient projection and particle swarm optimization(PSO) is presented. Then the rotation angles are obtained and the rotor position is identified. The validity of the sensing system is verified through the simulation.

**Keywords**: Halbach array, PMSM, 3-D hall sensor, PSO, Gradient projection method

## 1. Introduction

Multiple degrees of freedom (DOF) manipulators are widely used in the area where their end-effectors must be positioned rapidly, smoothly and precisely, such as the application and research fields of intelligent robotics, military, industrial automation, modern aviation and aerospace, etc. Traditionally, multi-DOF is implemented by a couple of single DOF motors with complex mechanical transmission mechanism, which causes complexity in mechanical structure, bulkiness in volume, slow responses, low positioning precision and dynamic performance. All these factors contribute to the development of spherical motor, which can provide up to 3 DOF independently, greatly simplifying mechanical structure and improving precision and response speed [1-2].

In close-loop control system, position sensing system of the motor is necessary. However, PMSM is still at the starting stage, facing many challenges, especially in the position sensing system. So far, many efforts to form an efficient and reliable sensing system have been made. A fast response and high accuracy sensing systems is achieved by three optical encoders and two guides [3]. However, the use of guides and optical encoders increases the volume of the motor and introduces additional inertia and friction that can affect the dynamic performance and control performance of the motor. Optical sensors have been successfully applied to obtain the rotor position [4]. In [5], the rotor orientation is achieved by detecting the states which are decided by the rotor sphere surface's color. However, a strict working environment is needed in these two kinds of position detection methods. What's more, various kinds of multi-DOF detecting techniques and methods (such as, inertia/gyroscopic sensors, laser interferometers [6], vision-based [7], were put forward. However, these sensing systems have a common fatal defect that their volume increase a lot which damages the PMSM's control performances. Magnetic field solutions are favored by researches, which have the advantage of passivity, permeability, invariance to environmental factors and free of 'line of sight' requirement [8]. In [9], an artificial neural network was established between measured field and position information to obtain rotor position. However, there is a tradeoff between its speed and precision. In [10], the position of the rotor was detected by six uniaxial hall sensors and optical sensors. However, the position detection accuracy was relatively low due to the high harmonics of the rotor magnetic field were neglected. With the development of 3-D hall sensor, three components of the magnetic field can be easily acquired and detected precisely [11-12]. In [13], the rotor position is obtained by solving the equations established between the rotor magnetic field and the position information through a nonlinear optimization algorithm. However, this method is relatively slow and requires a good initial search point. In addition, this paper neglects the influence of the rotor magnetic field harmonics and the magnetic field generated by the stator coil on position detection.

In this paper, a further study is carried out based on [13]. In order to get rid of the influence on the position detection

† Corresponding Author: Dept. of Electrical Engineering and Automation, Tianjin University, China. (liu_wen_jun@tju.edu.cn)
* Dept. of Electrical Engineering and Automation, Tianjin University, China. ({lihongfeng, elib}@tju.edu.cn)
Received :May 11, 2017 ; Accepted: October 24,2017

caused by the harmonics of rotor magnetic field and the stator coil magnetic field, a sensor location combination scheme was proposed. The relationship between the rotation angles and the measured magnetic flux density is nonlinear and serious coupling, which resulting in the complexity of the inverse computing. Based on this, a new position solution algorithm which combines the merits of gradient projection and particle swarm optimization was presented. Then the rotor position can be identified fast and accurately.

## 2. Position Identification Method

The structure and principle of a PMSM are introduced in [13-15], and Fig. 1 shows the schematic diagram of the motor's 3 DOF motion, where Figs. 1a–1c signify spinning, yawing and pitching motion respectively.

Position feedback signals are essential in close-loop control system. 3-D hall sensor can export 3 components which are proportional to the magnet flux density. In order to study the magnetic field distribution and depict the motion of rotor, $\Sigma(XYZ), \Sigma(R\Theta\Phi), \Sigma(dqp), \Sigma(r\theta\varphi)$ (which denotes stator rectangular coordinate system, stator spherical coordinate system, rotor rectangular coordinate system and rotor spherical coordinate system respectively) are defined, as illustrated in Fig. 2.

### 2.1 Magnetic field distribution

The paper shows that Halbach array permanent magnet spherical motor has a good performance in reducing harmonic components of the magnetic field [14]. Besides, the magnet flux density of a 4 poles motor in the $\Sigma(r\theta\varphi)$ is presented by [14].

$$\begin{bmatrix} B_r \\ B_\theta \\ B_\varphi \end{bmatrix} = \begin{bmatrix} k_r r^{-4} \cos(2\varphi)\sin^2\theta \\ k_\varphi r^{-4} \sin(2\varphi)\sin\theta \\ k_\theta r^{-4} \cos(2\varphi)\sin(2\theta) \end{bmatrix} \quad (1)$$

Where $k_r, k_\theta, k_\varphi$ are only up to the PMSM's property and structure of permanent magnet, and their expressions are shown in Appendix. r denotes the distance to rotor's centre.

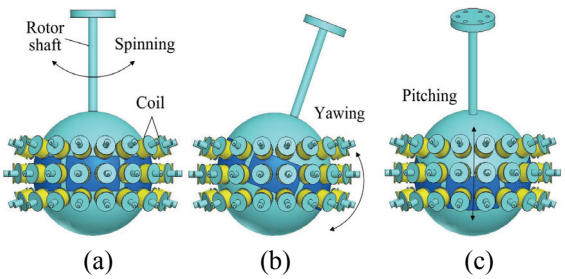


**Fig. 1** The schematic diagram of the 3 DOF motion

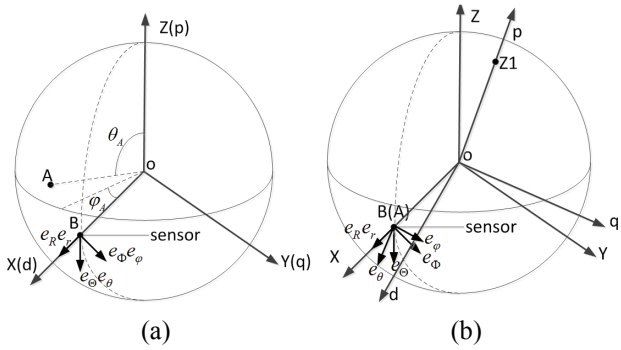


**Fig. 2** The sketch map of positioning

### 2.2 Positioning process

At the initial moment the rotor shaft is vertical with the X-Y plane of the stator, $\Sigma(XYZ)$ coincides with $\Sigma(dqp)$, as illustrated in Fig.2a.The 3-D hall sensor is installed on the point B(as the main sensor), whose stator spherical coordinate simply notes as $(R_0, 90^\circ, 0^\circ)_{R\Theta\Phi}$ located on the stator of the PMSM, where the subscript $R\Theta\Phi$ represents $\Sigma(R\Theta\Phi)$ and $R_0$ denotes the distance to rotor's centre. In this paper, the width of the air gap is ignored, the radius of the stator ball and the rotor ball is unified denoted as $R_0$. $B_R, B_\Theta$ and $B_\Phi$ are 3 components of magnetic flux density in the $\Sigma(R\Theta\Phi)$. A is a point located in the air gap, whose coordinates are $(R_0, \theta_A, \varphi_A)_{R\Theta\Phi}$ and $(R_0, \theta_A, \varphi_A)_{r\theta\varphi}$, where $\theta_A$ and $\varphi_A$ are unknown. When point A rotates to the point B, the rotor shaft will get to $Z_1$ at the same time, as illustrated in Fig. 2b.

Although the motion track from point A to point B is unknown, this process can be implemented by three rotation transformations which rotate around each axis of $\Sigma(XYZ)$. The rotation angles around X, Y and Z axes are $\alpha_A$, $90^\circ - \theta_A$ and $-\varphi_A$ separately, where $\alpha_A$ is uncharted. Similarly, the rotor shaft from the initial position to $Z_1$ undergoes the same changes. The three angles of this rotation around X, Y and Z are defined as $\alpha, \beta$ and $\gamma$ respectively. Due to the point A and the rotor shaft is a whole, the relationship between the two group rotation angles is as follows.

$$\begin{cases} \alpha = \alpha_A \\ \beta = 90^\circ - \theta_A \\ \gamma = -\varphi_A \end{cases} \quad (2)$$

The coordinate of the point $Z_1$ in the stator coordinate system after rotation is given by Eq. (3):

$$\begin{bmatrix} X_{Z_1} & Y_{Z_1} & Z_{Z_1} \end{bmatrix}^T = \boldsymbol{C}_1 \times \boldsymbol{C}_2 \times \boldsymbol{C}_3 \times \begin{bmatrix} 0 & 0 & R_0 \end{bmatrix}^T \quad (3)$$

Where $\boldsymbol{C}_1$, $\boldsymbol{C}_2$ and $\boldsymbol{C}_3$ are rotation matrices correspond

to the above three rotations, respectively.

$$\boldsymbol{C}_1 = \begin{bmatrix} 1 & 0 & 0 \\ 0 & \cos\alpha & \sin\alpha \\ 0 & -\sin\alpha & \cos\alpha \end{bmatrix} \tag{4}$$

$$\boldsymbol{C}_2 = \begin{bmatrix} \cos\beta & 0 & -\sin\beta \\ 0 & 1 & 0 \\ \sin\beta & 0 & \cos\beta \end{bmatrix} \tag{5}$$

$$\boldsymbol{C}_3 = \begin{bmatrix} \cos\gamma & \sin\gamma & 0 \\ -\sin\gamma & \cos\gamma & 0 \\ 0 & 0 & 1 \end{bmatrix} \tag{6}$$

The coordinate of the rotor shaft in $\Sigma(R\Theta\Phi)$ is given as:

$$\begin{aligned} \Theta_{Z_1} &= \arccos(Z_{Z_1} / R_0) \\ \Phi_{Z_1} &= \arctan(Y_{Z_1} / X_{Z_1}) \end{aligned} \tag{7}$$

It is obvious that if the rotation angles involved in Eq. (3) and (7) are solved, the rotor position should be achieved.

### 2.3 Magnetic field model of main magnetic field sensor

According to the magnetic flux density vector relationship between $\Sigma(R\Theta\Phi)$ and $\Sigma(dqp)$ shown in Fig. 2 and the vector projection principle, the equation is obtained as follows:

$$\begin{cases} B_R = B_r \\ B_\Theta = B_\theta \cos(\alpha_\Lambda) - B_\varphi \sin(\alpha_\Lambda) \\ B_\Phi = B_\theta \sin(\alpha_\Lambda) + B_\varphi \cos(\alpha_\Lambda) \end{cases} \tag{8}$$

Using (1), (2) and (8) becomes:

$$\begin{cases} B_R = k_r r^{-4} \cos(2\gamma)\cos^2\beta \\ B_\Theta = k_\theta r^{-4} \cos(2\gamma)\sin(2\beta)\cos\alpha \\ \quad + k_\varphi r^{-4} \sin(2\gamma)\cos\beta\sin\alpha \\ B_\Phi = k_\theta r^{-4} \cos(2\gamma)\sin(2\beta)\sin\alpha \\ \quad - k_\varphi r^{-4} \sin(2\gamma)\cos\beta\cos\alpha \end{cases} \tag{9}$$

## 3. Solutions to Get Rid of the Influence Factors on Position Detection

Although the harmonics in PMSM decreases a lot with the application of Halbach array, harmonic component will still affect the magnetic flux density on the testing point, which will lower position detection accuracy. In addition, magnetic field of the stator coil will produce certain effect on the position detection. Therefore, it is necessary to find feasible methods to avoid the impact of these factors on the rotor position detection. This paper takes an electric current 10A, 200 coils of stator windings as an example to analyze, and one point of the stator windings is selected to observe the variation of its surrounding magnetic field. This paper selects a point whose spherical coordinate of the stator windings is $\varphi$=3°, $\theta$=85° to analyze, and its magnetic field along with the change of the distance $r$ is shown in Fig. 3.

Fig.3. show that the nearer to the stator coil, the bigger value of each component of the magnetic field is. The magnetic field exists only in the vicinity of the selected point and the magnetic field value quickly declines to zero with the distance $r$ increases. The paper shows that the harmonic components in the Halbach array PMSM are very small [15]. Based on all factors discussed above, solutions to get rid of the influence on the position detection caused by the harmonics of rotor magnetic field and the stator coil magnetic field are proposed. The main idea is that a magnetic field threshold is chosen, whose value is larger than the sum of the amplitude of the harmonics of rotor magnetic field and the stator coil magnetic field. In this paper, the threshold value is set as 0.01T, which has sufficient margin. Besides, one or several auxiliary magnetic field sensors are needed. When the magnetic field value detected by the main sensor is below the threshold, the magnetic field value detected by the auxiliary sensor is adopted.

The installation of the auxiliary sensors needs to meet the following principles:

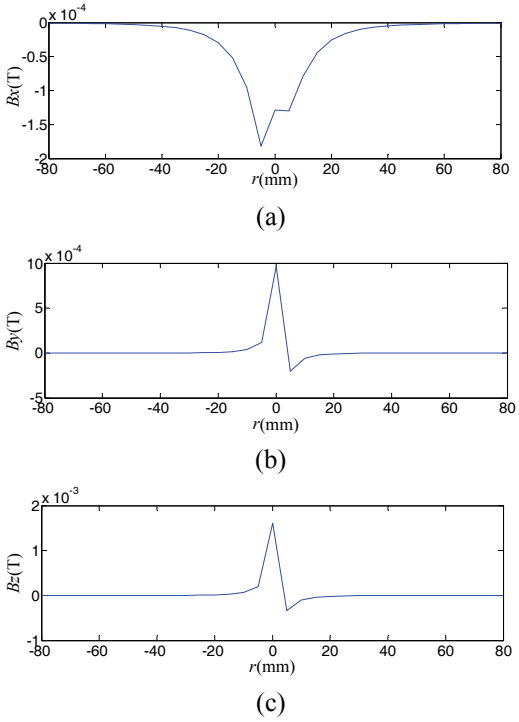


**Fig. 3** The magnetic field of the stator coil with distance $r$ varies

1) Due to the symmetry of the spherical motor, the installation position of the auxiliary sensor is within the MPNM plane (as shown in Fig. 6) or its projection is in the MPNM plane.

2) The area where the magnetic field detected by the auxiliary sensor falls below the threshold value needs to be staggered from the area where the main sensor and the other auxiliary sensors detected.

3) In the range of values of $\alpha,\beta,\gamma$, at least one of $B_R(\alpha,\beta,\gamma)$, $B_{R1}(\alpha,\beta,\gamma)$ … $B_{Rn}(\alpha,\beta,\gamma)$ is bigger than the threshold. At least one of $B_\Theta(\alpha,\beta,\gamma)$, $B_{\Theta1}(\alpha,\beta,\gamma)$ … $B_{\Theta n}(\alpha,\beta,\gamma)$ is bigger than the threshold. At least one of $B_\Phi(\alpha,\beta,\gamma)$, $B_{\Phi1}(\alpha,\beta,\gamma)$ … $B_{\Phi n}(\alpha,\beta,\gamma)$ is bigger than the threshold.

Where $B_R(\alpha,\beta,\gamma)$, $B_\Theta(\alpha,\beta,\gamma)$, $B_\Phi(\alpha,\beta,\gamma)$ and $B_{Rn}(\alpha,\beta,\gamma)$, $B_{\Theta n}(\alpha,\beta,\gamma)$, $B_{\Phi n}(\alpha,\beta,\gamma)$ denotes the three magnetic field components of the main sensor and the three magnetic field components of the *n*-th auxiliary sensor, respectively.

The magnetic field of the main sensor is shown in Eq. (9). It can be found that $B_R$, $B_\Theta$ and $B_\Phi$ are periodic with respect to $\gamma$ and the period is 180°. In addition, due to the limitation of mechanical structure, the titling motion angle of spherical motor is finite. In this paper, the motion angle is less than 45°.So -45°<$\alpha$<45°, -45°<$\beta$<45°, -90°<$\gamma$<90° will be determined.

Principle 2) actually requires the auxiliary sensor configuration is to rotate the main sensor around the three axes of $\Sigma(XYZ)$ about $\Delta\alpha$, $\Delta\beta$, $\Delta\gamma$ respectively. The magnetic field detected by auxiliary magnetic field sensor is shown as follows:

$$\begin{cases} B_R = k_r r^{-4}\cos(2(\gamma-\Delta\gamma))\cos^2(\beta-\Delta\beta) \\ B_\Theta = k_\theta r^{-4}\cos(2(\gamma-\Delta\gamma))\sin(2(\beta-\Delta\beta))\cos(\alpha-\Delta\alpha) \\ \quad + k_\varphi r^{-4}\sin(2(\gamma-\Delta\gamma))\cos(\beta-\Delta\beta)\sin(\alpha-\Delta\alpha) \\ B_\Phi = k_\theta r^{-4}\cos(2(\gamma-\Delta\gamma))\sin(2(\beta-\Delta\beta))\sin(\alpha-\Delta\alpha) \\ \quad - k_\varphi r^{-4}\sin(2(\gamma-\Delta\gamma))\cos(\beta-\Delta\beta)\cos(\alpha-\Delta\alpha) \end{cases} \quad (10)$$

The possible rotation angle $\Delta\alpha$ is chosen as [-45° (initial): 5°(interval): 45°(final)], $\Delta\beta$ is chosen as [-45°: 5°: 45°], $\Delta\gamma$ is chosen as [-90°:5°:90°].

In order to find the optimal configuration of the magnetic field sensor, we need to make full use of each sensor and to avoid getting repetitive information from different sensors as much as possible, namely, the bigger the difference between each sensor, the better performance of the sensor combination will be. Based on this, the difference function T is defined as following:

$$T_1=(B_{R1}-B_R)^2+(B_{\Theta1}-B_\Theta)^2+(B_{\Phi1}-B_\Phi)^2 \quad (11)$$

It is calculated that when $\Delta\alpha$=0°, $\Delta\beta$=0°, $\Delta\gamma$=45°, $T_1$ reaches the maximum, so the installation location of auxiliary sensor 1 will be determined by rotating the main sensor position around the three axes of $\Sigma(XYZ)$ about 0 °, 0°, 45° respectively. When $\alpha$=2° and $\gamma$=90°, the absolute values of the $B_\Theta$ component of the main magnetic field sensor and the auxiliary magnetic field sensor 1 are shown in Fig. 4. It can be seen that in some specific areas the magnetic field detection value of the auxiliary magnetic field sensor 1 is also lower than the detection threshold when the $B_\Theta$ component of the main sensor is lower than the detection threshold, which does not satisfy the principle 3). In other words, the addition of the auxiliary sensor 1 did not achieve full coverage of the rotor workspace, so the second auxiliary magnetic field sensor is needed.

The difference function for finding the second auxiliary magnetic field sensor is defined as follows:

$$T_2=(B_{R2}-B_R)^2+(B_{\Theta2}-B_\Theta)^2+(B_{\Phi2}-B_\Phi)^2+(B_{R2}-B_{R1})^2 +(B_{\Theta2}-B_{\Theta1})^2+(B_{\Phi2}-B_{\Phi1})^2 \quad (12)$$

It is calculated that when $\Delta\alpha$=45°, $\Delta\beta$=45°, $\Delta\gamma$=-90°, $T_2$ reaches the maximum, so the installation location of auxiliary sensor 2 will be determined by rotating the main sensor position around the three axes of $\Sigma(XYZ)$ about 45°, 45°, -90° respectively. When $\alpha$ = 2 ° and $\gamma$ = 90 °, the absolute values of the $B_\Theta$ component of the main magnetic field sensor and the auxiliary magnetic field sensor 1,2 are shown in Fig. 5. As can be seen from Fig. 5, when magnetic field detection value of the main sensor and the auxiliary sensor 1 are below the detection threshold, the detection value of the auxiliary sensor 2 is higher than the detection threshold.

The installation location of the main sensor and auxiliary sensors is shown in Fig. 6. In order to verify whether the sensor location combination scheme can achieve the full coverage of the rotor workspace, a flag variable *Flag* is defined in this paper.

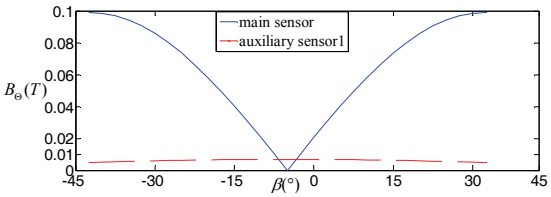


**Fig. 4** The comparison of rotor magnetic field between the main magnetic field sensor and the auxiliary magnetic field sensor 1

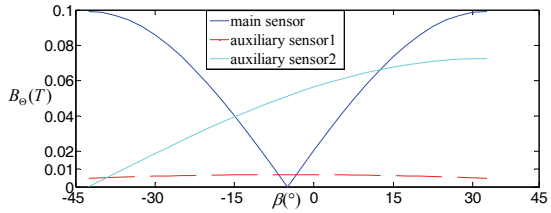


**Fig. 5** The comparison of rotor magnetic field between the main magnetic field sensor and the auxiliary magnetic field sensor 1,2

In the range of values of $\alpha,\beta,\gamma$, if principle 3) is satisfied, *Flag*=1, otherwise *Flag*=0. The test samples are set as follows: $\alpha$= [-45°:0.01°:45°],$\beta$= [-45°:0.01°:45°],$\gamma$=[-90°:0.01°:90°]. The test result shows that *Flag* is always equal to 1. In other words, the sensor location combination scheme can achieve the full coverage of the rotor workspace.

$\alpha$=30°, $\gamma$=87.5° is taken to serve as an example. The absolute value image of $B_R$, $B_\Theta$, $B_\Phi$ detected by the main sensor and the auxiliary sensors is shown in Fig. 7.

Fig. 7 shows that in some areas the magnetic field detection value of the main sensor is smaller than the detection threshold, but in these areas the magnetic field detection value in one or two auxiliary sensors can always be found to be larger than the detection threshold. When $\alpha,\beta$ and $\gamma$ are assigned any values within the constraint range, the same conclusion will be always obtained by using the proposed sensor location combination scheme. In other words, the proposed method to avoid the influence of the rotor magnetic field harmonics and the stator coil magnetic field on the position detection is effective.

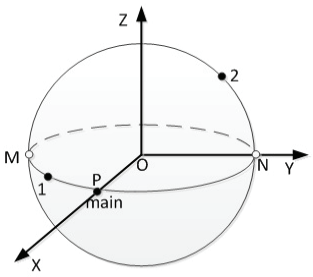


**Fig. 6** The installation location map of the main magnetic field sensor and the auxiliary magnetic field sensors

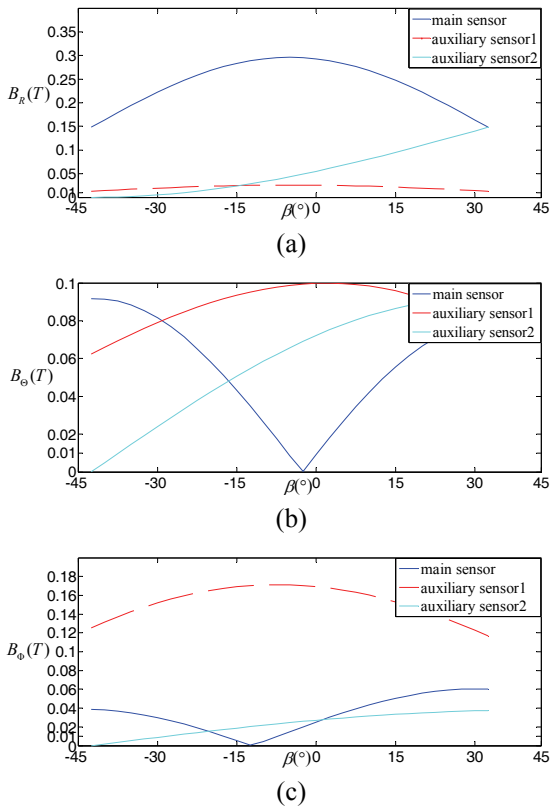


**Fig. 7** The comparison of rotor magnetic field between the main magnetic field sensor and the auxiliary magnetic field sensor 1,2

## 4. Position Solution Algorithm

As discussed above, the relationship between the rotation angles and the measured magnetic flux is nonlinear and serious coupling. It is needed to seek for the corresponding algorithm to solve this equation so as to obtain the position information of the PMSM. A new position solution algorithm which combines the strengths of both gradient projection and particle swarm optimization is proposed in this paper and proved practicable in obtaining a fast response and high accuracy sensing systems.

### 4.1 Fitness function

In order to avoid the influence of the rotor magnetic field harmonics and the stator coil magnetic field on the position detection, it is necessary to consider the value of the auxiliary sensor when any component of the magnetic field detected by the main sensor is below the threshold. All magnetic field sensors considered, the magnetic field model in the $\Sigma(R\Theta\Phi)$ is shown as follows.

$$\begin{cases} B_{Ri} = k_r r^{-4}\,\mathrm{c}(2(\gamma-\Delta\gamma_i))\,\mathrm{c}^2(\beta-\Delta\beta_i) \\ B_{\Theta i} = k_\theta r^{-4}\,\mathrm{c}(2(\gamma-\Delta\gamma_i))\,\mathrm{s}(2(\beta-\Delta\beta_i))\,\mathrm{c}(\alpha-\Delta\alpha_i) \\ \quad + k_\varphi r^{-4}\,\mathrm{s}(2(\gamma-\Delta\gamma_i))\,\mathrm{c}(\beta-\Delta\beta_i)\,\mathrm{s}(\alpha-\Delta\alpha_i) \\ B_{\Phi i} = k_\theta r^{-4}\,\mathrm{c}(2(\gamma-\Delta\gamma_i))\,\mathrm{s}(2(\beta-\Delta\beta_i))\,\mathrm{s}(\alpha-\Delta\alpha_i) \\ \quad - k_\varphi r^{-4}\,\mathrm{s}(2(\gamma-\Delta\gamma_i))\,\mathrm{c}(\beta-\Delta\beta_i)\,\mathrm{c}(\alpha-\Delta\alpha_i) \end{cases} \tag{13}$$

Where $i$=0 represents the main sensor, $i$=1, 2 represents the $i$-th auxiliary sensor, s=sin, c=cos.

$$\begin{aligned} &\Delta\alpha_0 = \Delta\beta_0 = \Delta\gamma_0 = \Delta\alpha_1 = \Delta\beta_1 = 0^\circ, \\ &\Delta\gamma_1 = \Delta\alpha_2 = \Delta\beta_2 = 45^\circ, \Delta\gamma_2 = -90^\circ \end{aligned} \tag{14}$$

$f_{1i}(\alpha,\beta,\gamma)$, $f_{2i}(\alpha,\beta,\gamma)$ and $f_{3i}(\alpha,\beta,\gamma)$ are defined as follows.

$$\begin{cases} f_{1i} = B_{Ri} - k_r r^{-4}\,\mathrm{c}(2(\gamma-\Delta\gamma_i))\,\mathrm{c}^2(\beta-\Delta\beta_i) \\ f_{2i} = B_{\Theta i} - k_\theta r^{-4}\,\mathrm{c}(2(\gamma-\Delta\gamma_i))\,\mathrm{s}(2(\beta-\Delta\beta_i))\,\mathrm{c}(\alpha-\Delta\alpha_i) \\ \quad - k_\varphi r^{-4}\,\mathrm{s}(2(\gamma-\Delta\gamma_i))\,\mathrm{c}(\beta-\Delta\beta_i)\,\mathrm{s}(\alpha-\Delta\alpha_i) \\ f_{3i} = B_{\Phi i} - k_\theta r^{-4}\,\mathrm{c}(2(\gamma-\Delta\gamma_i))\,\mathrm{s}(2(\beta-\Delta\beta_i))\,\mathrm{s}(\alpha-\Delta\alpha_i) \\ \quad + k_\varphi r^{-4}\,\mathrm{s}(2(\gamma-\Delta\gamma_i))\,\mathrm{c}(\beta-\Delta\beta_i)\,\mathrm{c}(\alpha-\Delta\alpha_i) \end{cases} \tag{15}$$

When $B_{R0}<0.01$, let $f_1=\max(|f_{1i}|)$; when $B_{\Theta 0}<0.01$, let $f_2=\max(|f_{2i}|)$; when $B_{\Phi 0}<0.01$, let $f_3=\max(|f_{3i}|)$.

Then defines fitness function

$$F=\sum_{i=1}^{3} f_i^2, i=1,2,3 \tag{16}$$

It is obvious that the problem of the rotor position identification becomes an optimization problem. It can be seen from Eq. (1) that the Halbach array PMSM's rotor magnetic field distribution is symmetrical about the equator of rotor. Hence, it can't distinguish the area between $\theta_A<\pi/2$ and $\theta_A>\pi/2$ merely by using 3-D hall sensor. It is easily found that the position command $\Phi_{Z_1}$ determines the region of $\theta_A$. If the orientation command is $0<\Phi_{Z_1}<\pi/2$ or $3\pi/2<\Phi_{Z_1}<2\pi$, point A located on the upper hemisphere will rotate to point B as shown in Fig. 2, namely $\theta_A<\pi/2$. Similarly, if the orientation command is $\pi/2<\Phi_{Z_1}<3\pi/2$, the conclusion that $\theta_A>\pi/2$ will be obtained. In addition, since the motion of the rotor is limited by the mechanical structure of the motor, the position detection problem in this paper becomes a constrained optimization problem. The fitness function is defined as follows.

$$\begin{cases} \min F=\min(\sum_{i=1}^{3} f_i^2) \\ -\pi/4<\alpha<\pi/4 \\ -\pi/4<\beta<\pi/4 \\ -\pi/2<\gamma<\pi/2 \end{cases} \tag{17}$$

However, traditional methods have difficulty in solving this problem quickly. Base on this situation, a new position solution algorithm is proposed as follows.

### 4.2 Position solution algorithm

Due to the problem of the rotation angles obtained from measured magnetic field is similar to the problem of the robot's reverse kinematics, gradient projection method which is widely used in robot's area is attempted in this paper. Calculate the derivation of the Eq. (15), so as to get the Eq. (18).

$$\dot{\boldsymbol{B}}=\boldsymbol{J}\dot{\boldsymbol{\theta}} \tag{18}$$

where $\boldsymbol{B}=[B_R \quad B_\Theta \quad B_\Phi]^{\mathrm{T}}$, $\boldsymbol{\theta}=[\alpha \quad \beta \quad \gamma]^{\mathrm{T}}$.

According to the Liegeois gradient projection method, a general solution form is given as follows:

$$\begin{cases} \dot{\boldsymbol{\theta}}=\dot{\boldsymbol{\theta}}_p+\dot{\boldsymbol{\theta}}_h=\boldsymbol{J}^{+}\dot{\boldsymbol{F}}+(\boldsymbol{I}-\boldsymbol{J}^{+}\boldsymbol{J})\dot{\boldsymbol{\varphi}} \\ \boldsymbol{J}^{+}=\boldsymbol{J}^{\mathrm{T}}(\boldsymbol{J}\boldsymbol{J}^{\mathrm{T}})^{-1} \\ \dot{\boldsymbol{\theta}}_p=\boldsymbol{J}^{+}\dot{\boldsymbol{B}} \\ \dot{\boldsymbol{\theta}}_h=(\boldsymbol{I}-\boldsymbol{J}^{+}\boldsymbol{J})\dot{\boldsymbol{\varphi}} \end{cases} \tag{19}$$

Where $\boldsymbol{J}^{+}$ is the generalized inverse matrix of Jacobi matrix, $\dot{\boldsymbol{\theta}}_p$ is the minimum norm solution, $\dot{\boldsymbol{\theta}}_h$ is the homogeneous solution, $\dot{\boldsymbol{\varphi}}$ is the rotation angles' velocity vector, $\boldsymbol{I}-\boldsymbol{J}^{+}\boldsymbol{J}$ is projection matrix of the Zero space.

Eq. (16) is the fitness function of the gradient projection method. Eq. (20) is obtained by introducing the velocity vector of the rotor rotation angle.

$$\dot{\boldsymbol{\varphi}}=k\cdot\nabla F(\boldsymbol{\theta}) \tag{20}$$

Where $\nabla F(\boldsymbol{\theta})$ is the gradient vector of the optimization objective function, $k$ is the proportion amplification coefficient, conventionally, $k$ ranges from -1 to 1, when $k<0$ the minimum objective function will be achieved. So the equation becomes:

$$\dot{\boldsymbol{\theta}}=\boldsymbol{J}^{+}\dot{\boldsymbol{B}}+k(\boldsymbol{I}-\boldsymbol{J}^{+}\boldsymbol{J})\nabla F(\boldsymbol{\theta}) \tag{21}$$

15 sets of rotation angles are given firstly. The position command in the $\Sigma(R\Theta\Phi)$ will be obtained subsequently according to rotation transformation theory. Then the rotation angles will be solved by using the gradient projection algorithm. The actual rotation angles and solved rotation angles are illustrated in the same image, as shown in Fig. 8.Where Figs. 8a-8c demonstrate the rotation angles $\alpha$, $\beta$ and $\gamma$ separately. The blue line and the red line denote

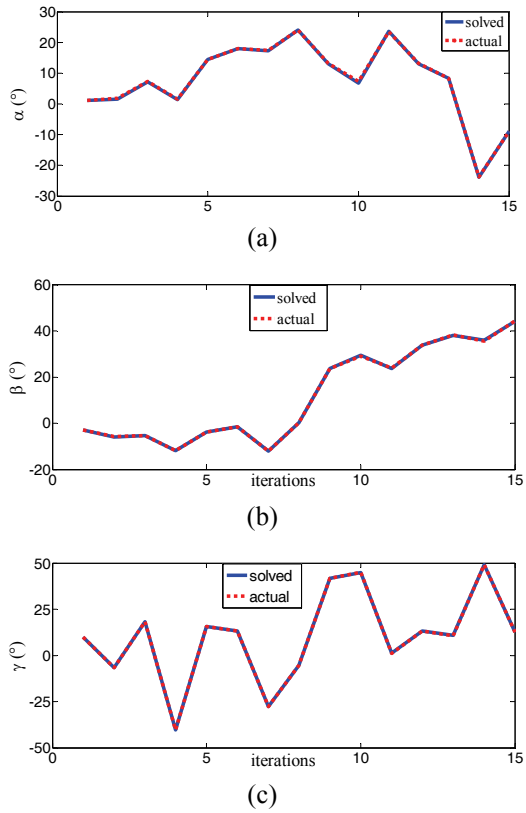


**Fig. 8** The comparison of rotation angles solved by gradient projection and actual rotation angles

the solved rotation angles and the actual rotation angles, separately. It shows that the gradient projection is very accurate. However, this algorithm will be relatively slow if the initial searching point is not proper. If an approximate optimal solution is employed to serve as initial searching point, the gradient projection can achieve a high precision and a fast convergence.

Furthermore, this paper selects the rotation angles with different fitness as the initial point of the gradient projection method and records its computing time. The relationship between the computing time of the gradient projection and the initial point's fitness is shown in Fig. 9. It shows that computing time has no definite function relation with the fitness of the initial point. But an initial point with big fitness is apt to consume more time. Especially, when the fitness of the initial point is more than 0.01, the calculate speed turns slow obviously.

In order to obtain a good initial searching point for the gradient projection, this paper studies particle swarm optimization. The particle swarm algorithm is designed according to [16]. Similarly, Eq. (16) is the fitness function of this PSO algorithm. Fig. 10 shows the variation of the fitness function as the number of iterations increases. The fitness of rotation angles obtained by particle swarm algorithm is less than 0.01 and even can reach 0.001. However, in some high accuracy requirement field, this PSO algorithm can't meet it. But the approximate optimal solution obtained by PSO is suitable used as the initial point of the gradient projection method, then the solving speed can be speeded up.

As discussed above, the gradient projection has very high precision, but the computing speed of this algorithm will be very slow if the initial searching point is not proper. The particle swarm optimization has quick computing speed, but its precision is relatively low. Naturally, a new algorithm was born which combines the strengths of both gradient projection and particle swarm optimization. Firstly, an approximate optimal solution was obtained by using the PSO algorithm. Subsequently, this optimal solution serves as the initial point of the gradient projection, then the high accurate solutions will be obtained quickly, i.e. the sensing system of the Halbach array permanent magnet spherical motor is verified.

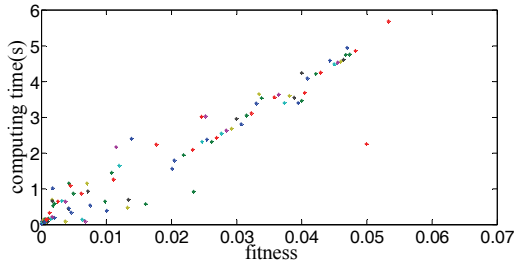


**Fig. 9** The relationship between the computing time of the gradient projection algorithm and the initial point's fitness

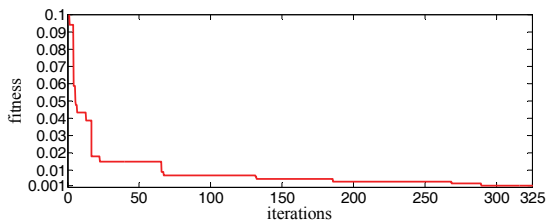


**Fig. 10** Iterative process

## 5. Simulation Experiment

### 5.1 Simulation process

The sensing system proposed in this paper is magnetic field-based, so magnetic field data is needed. Firstly, the stator spherical coordinate of rotor shaft is given. Secondly, the 3-D hall sensor's outputs are obtained by rotation transformation and the magnetic field model of Halbach array PMSM. Thirdly, the rotation angles are solved by using the combined algorithm presented in this paper. Finally, the stator spherical coordinate of rotor shaft is obtained by rotation transformation. The simulation diagram of position sensing system is shown in Fig. 11, where $\Theta^*$ and $\Phi^*$ are the given position command in $\Sigma(R\Theta\Phi)$, $\Theta$ and $\Phi$ are the measured position by sensing system.

### 5.2 Simulation result

In order to observe the effectiveness of this sensing system vividly, four simulation experiments are implemented in this paper. The position command in four experiments is given in $\Sigma(R\Theta\Phi)$. (i) $\Phi^*$ is 0, the initial value of $\Theta^*$ is $\pi/60$, $\Theta^*$ increases by $\pi/60$ every sampling time. (ii) $\Phi^*$ is $\pi/2$, the initial value of $\Theta^*$ is $\pi/60$, $\Theta^*$ increases by $\pi/60$ every sampling time.(iii) $\Theta^*$ s $\pi/4$, the initial value of $\Phi^*$ is $\pi/15$, $\Phi^*$ increases by $\pi/15$ every sampling time. (iv) The initial value of $\Theta^*$ s $\pi/60$, $\Theta^*$ increases by $\pi/60$ every sampling time, the initial value of $\Phi^*$ is $\pi/15$, $\Phi^*$ increases by $\pi/15$ every sampling time. In this way, 25 sets of data are selected and the trajectory is figured in each experiment. In addition, the desired trajectory and the tracking trajectory

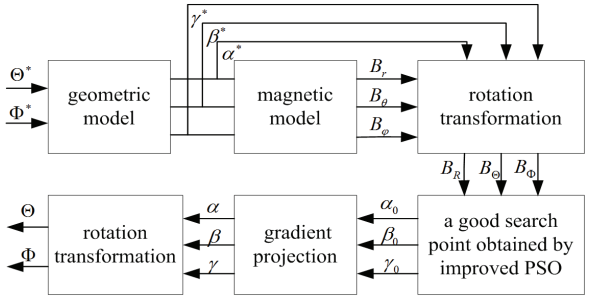


**Fig. 11** Simulation diagram of position sensing system

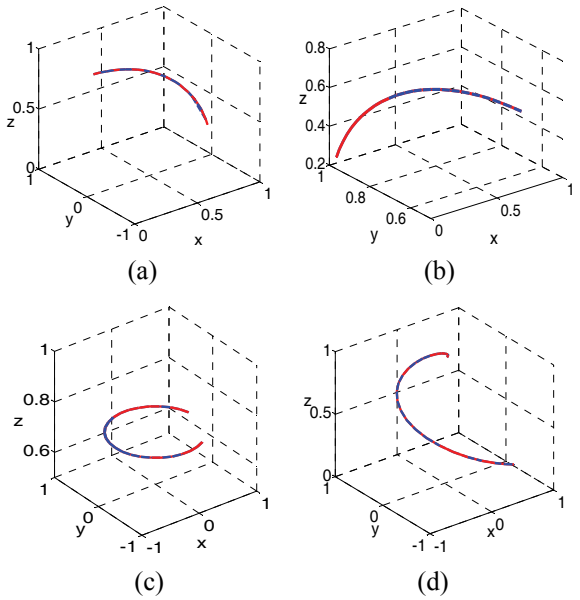


**Fig. 12** The comparison of trajectory of desired and tracking with the proposed algorithm

**Table 1.** Performance of proposed algorithm

| No. | 1 | 2 | 3 | 4 |
|---|---|---|---|---|
| execution time (s) | 34.1055 | 39.4558 | 31.6537 | 35.4427 |
| average execution time (s) | 1.36422 | 1.57823 | 1.26615 | 1.41771 |

are compared in the same figure. The simulation results are shown in Figs. 12(a)-12(d) separately.

The blue line and the red line denote the desired trajectory and the tracking trajectory, separately. Fig. 12 shows that the identified position has very small error with the actual position, namely, the sensing system presented in this thesis is effective.

At the same time, the execution time of four experiments is counted, and the average execution time of one set of data in each experiment is calculated. The result is depicted in Table 1.

From Table 1, we can see that the proposed algorithm has a shorter execution time, which proves that the position detection method proposed in this paper is fast.

### 5.3 Simulation result by finite element model method

As shown above, the proposed sensing system has an excellent performance in obtaining the rotor position. However, the magnet model is ideal. Following works are conducted to verify that if the magnetic field data is from a finite element model(FEM), can the detection method be still feasible?

Firstly, 3-D FEM of the Halbach array PMSM is built in Ansoft Maxwell 15.0, as shown in Fig. 13(a). The Halbach array magnetization direction is shown in Fig. 13(b). In the $\Sigma(r\theta\varphi)$, $\theta = 60^\circ$, $r = 50\text{mm}$ is set, and the magnetic field distribution changing with the angle $\varphi$ is taken for

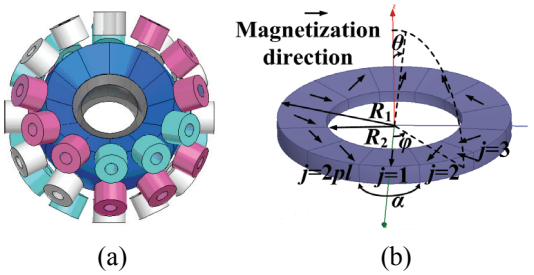


**Fig. 13** 3-D FEM of the Halbach array PMSM and the Halbach array magnetization direction

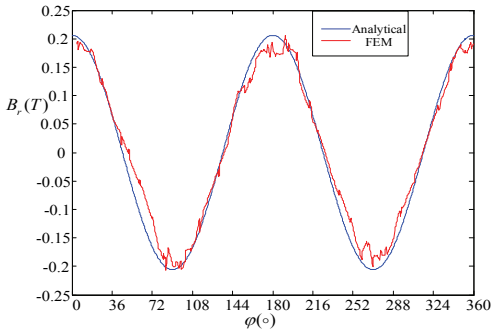


**Fig. 14.** Comparison of the magnetic field distributions obtained by analytical method and FEM method

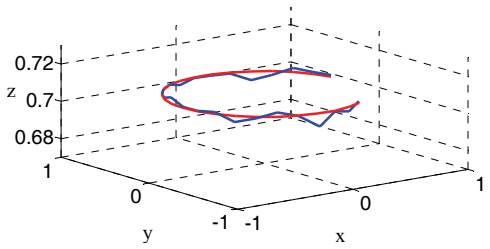

**Fig. 15** The comparison trajectory of desired and tracking with the proposed algorithm

an example to observe the performance of Halbach array in improving the magnetic field waveform. The magnetic field distributions of $B_r$ obtained by analytical method and FEM method are compared in Fig. 14.

Fig. 14 shows that the analytical method is in good agreement with the magnetic field distribution obtained by FEM. But there are still unavoidable errors between analytical method and FEM method. In order to further verify the feasibility of the detection method, the simulation experiment based on FEM magnetic field data is carried out.

The position command of the simulation is given in the $\Sigma(R\Theta\Phi)$. Position command: $\Theta^*$ is $\pi/4$, the initial value of $\Phi^*$ is $\pi/15$, $\Phi^*$ increases by $\pi/15$ every sampling time. In this way, 25 sets of data are selected and the desired trajectory is figured. Then the actual position data are solved by the proposed algorithm in the premise of using FEM magnetic field data. Subsequently, the tracking trajectory is depicted. The desired trajectory and the tracking

trajectory are compared in Fig. 15. The red line and the blue line denote the desired trajectory and the tracking trajectory, separately.

As can be seen from Fig. 15, although there are some errors, the detection data is still able to roughly reflect the actual position. It's true that further study should be done to improve the detection precision of the PMSM.

## 6. Conclusion

In this paper, a position detection method based on rotor magnetic field distribution was proposed for Halbach array PMSM. A sensor location combination scheme was proposed to get rid of the influence on the position detection caused by the harmonics of rotor magnetic field and the stator coil magnetic field. The relationship between the 3-D hall sensors' output on detecting point and the rotation angles was acquired by the magnetic field distribution and rotation transformation, then the nonlinear equation was solved by the combined algorithm proposed in this paper and the position identification was achieved. Then the sensing system was verified by the simulation experiment.

## Acknowledgements

This work was supported by National Natural Science Foundation of China. (no. 51677130)

## Appendix

$$k_r = \frac{2.3184a_2c_{22}\left|\boldsymbol{B}_r\right|R_0^4(-5R_0R_i^4\mu_r+3R_0^5\mu_r+2R_0^5\mu_m+2R_i^5\mu_r-2R_i^5\mu_m)}{-6R_i^5\mu_m+6R_i^5\mu_r\mu_m+6R_i^5\mu_r-6R_i^5\mu_r^2+4R_0^5\mu_r\mu_m+6R_0^5\mu_m+9R_0^5\mu_r+6\mu_r^2R_0^5}$$

$$k_\theta = \frac{-0.7728a_2c_{22}\left|\boldsymbol{B}_r\right|R_0^4(-5R_0R_i^4\mu_r+3R_0^5\mu_r+2R_0^5\mu_m+2R_i^5\mu_r-2R_i^5\mu_m)}{-6R_i^5\mu_m+6R_i^5\mu_r\mu_m+6R_i^5\mu_r-6R_i^5\mu_r^2+4R_0^5\mu_r\mu_m+6R_0^5\mu_m+9R_0^5\mu_r+6\mu_r^2R_0^5}$$

$$k_\varphi = \frac{1.5456a_2c_{22}\left|\boldsymbol{B}_r\right|R_0^4(-5R_0R_i^4\mu_r+3R_0^5\mu_r+2R_0^5\mu_m+2R_i^5\mu_r-2R_i^5\mu_m)}{-6R_i^5\mu_m+6R_i^5\mu_r\mu_m+6R_i^5\mu_r-6R_i^5\mu_r^2+4R_0^5\mu_r\mu_m+6R_0^5\mu_m+9R_0^5\mu_r+6\mu_r^2R_0^5} \quad \text{(A.1)}$$

Where $a_2, c_{22}$ are fundamental component coefficient of the residual magnetization of the magnet. For our spherical motor, $a_2 = 3.1058$,

$$c_{22} = 0.0483(2\cos^2\frac{\beta}{2}\sin\beta+3\beta+3\sin\beta).$$

The structure specifications of our spherical motor are list in table 2.

**Table 2.** Structure specifications of PMSM

| $R_0$/mm | $R_i$/mm | $\beta$ /° | $\boldsymbol{B}_r$ /T | $\mu_r$ | $\mu_m$ | $r$/mm |
|---|---|---|---|---|---|---|
| 45.6 | 26.5 | 60 | 1 | 1.02 | 1 | 50 |

## References

H. J. Lee, H. J. Park, S. H. Won, G. H. Ryu, and J. Lee, "Improvements of Performance of Multi-DOF Spherical Motor by Doubled Air-gap Feature," *JEET*, vol. 8, no. 1, pp. 90-96, 2013.

N. Kasashima, K. Ashida, T. Yano, A. Gofuku, and M. Shibata, "Torque Control Method of an Electro-magnetic Spherical Motor Using Torque Map," *IEEE/ASME Trans. Mechatronics*, vol. 21, no. 4, pp. 2050-2060, 2016.

M. Hoshina, T. Mashimo, and S. Toyama, "Develop-ment of spherical ultrasonic motor as a camera actuator for pipe inspection robot," *in Proc. IEEE int. Conf. Intelligent Robots and Systems*, pp. 2379-2384, Dec. 2009.

K. M. Lee and D. Zhou, "A Real-Time Optical Sensor for Simultaneous Measurement of Three-DOF moions," *IEEE/ASME Trans. Mechatronics*, vol. 9, no. 3, pp. 499-507, 2004.

Y. Oner, E. Cetin, A.Yilanci, and H. K. Ozturk, "Design and performance evaluation of a photovoltaic sun-tracking system driven by a three-freedom spherical motor," *Int. J. Exergy*, vol. 6, no. 6, pp. 853-867, 2009.

P. M. Wheat, N. A. Marine, J. L. Moran, and J. D. Posner, "Rapid fabrication of bimetallic spherical motors," *Langmuir*, vol. 26, no. 16, pp. 13052-13055, 2016.

H. Garner, M. Klement, and K.-M. Lee, "Design and analysis of an absolute non-contact orientation sensor for wrist motion control," *in Proc. IEEE int. Conf. Adv. Intell. Mechatronics*, pp. 69-74, July 2001.

S. H. Foong, K. M. Lee, and K. Bai, "Magnetic Field-based Sensing Method for Spherical Joint," *in Proc. IEEE int. Conf. Robotics and Automation*, pp. 5447-5452, May 2010.

J. J. Guo, C. Bak and H. Son, "Design of a Sensing System for a Spherical Motor Based on Hall Effect Sensors and Neural Networks," *in Proc. IEEE int. Conf. Advanced Intelligent Mechatronics*, pp. 1410-1414, July 2015.

H. Kawano, H. Ando, T. Hirahara, C. Yun and S. Ueha, "Application of a multi-DOF ultrasonic servo-motor in an auditory tele-existence robot," *IEEE Trans. Robotics,* vol. 21, no. 6, pp. 790-800, 2005.

P. Malcovati and F. Maloberti, "An Integrated Microsystem for 3-D Magnetic Field Measurements," *IEEE Trans. Instrumentation and Measurement*, vol. 49, no. 2, pp. 341-345, 2000.

D. X. CHEN, M. C. PAN, F. L. LUO, and W. Zhong, "The Design of a 3D Precision Magnetic Field Measurement System," *JTMT*, vol. 9, no. 3, pp. 279-282, 2005.

B. Li, C. L. Xia, H. F. Li and Y. Guan, "Study on the Position Identification of a Halbach Array Permanent Magnet Spherical Motor," *in Proc. IEEE int. Conf.*

*Robotics and Biomimetics*, pp. 2080-2084, Dec. 2007.
H. F. Li, C. L. Xia, P. Song, T. N. Shi, "Magnetic Field Analysis of A Halbach Array PM Spherical Motor," *in Proc. IEEE int. Conf. Automation and Logistics*, pp. 2019-2023, Aug. 2007.
H. F. Li, C. L. Xia, and T. N. Shi, "Spherical Harmonic Analysis of a Novel Halbach Array PM Spherical Motor," *in Proc. IEEE int. Conf. Robotics and Biomimetics*, pp. 2085-2089, Dec. 2007.
G. S. Chyan, S.G. Ponnambalam, "Obstacle avoidance control of redundant robots using variants of particle swarm optimization," *Journal of Robotics and Computer-Integrated Manufacturing*, vol. 28, no. 2, pp. 147-153, 2012.

**Hongfeng Li** She received the M.S. degree in intelligent control of electric drive systems and the Ph.D. degree in magnetic field analysis from Tianjin University, Tianjin, China, in 2005 and 2008, respectively. She is currently an Associate Professor in the School of Electrical Engineering and Automation, Tianjin University, Tianjin. Her current research interests include electrical machines, motor drives, and magnetic field analysis.

**Wenjun Liu** He is currently working toward the M.S. degree in electrical engineering from Tianjin University, China. His research interests include electrical machines, motor drives and control.

**Bin Li** He received the Ph.D. degree in electrical engineering from the Tianjin University, Tianjin, China, in 2006. From 2004 to 2009, he was a Lecturer in the School of Electrical Engineering and Automation, TJU. Since 2009, he has been an Associate Professor at TJU. As a Visiting Scholar, he was with the Department of Electrical Engineering and Computer Science, University of Central Florida, Orlando, FL, USA, from March 2014 to March 2015. His current research interests include electric machine design and control.